Exploring the Limits of High- T g Epoxy Vitrimers Produced through Resin-Transfer Molding

Vincent Schenk, Raffaele D'elia, Philippe Olivier, Karine Labastie, Mathias Destarac, Marc Guerre

Exploring the limits of high Tg epoxy vitrimers produced through resin transfer moulding

Vincent Schenk,[a,b,c] Raffaele D'Elia,[b] Philippe Olivier,[b,*] Karine Labastie,[a] Mathias Destarac[a,c] and Marc Guerre [c,*]

a. IRT Saint Exupéry, bâtiment B612 3 rue Tarfaya, 31405 Toulouse cedex 4, France.

b. ICA, Université de Toulouse, UT3, CNRS UMR 5312, Espace C. Ader, 3 Rue Caroline Aigle, 3140 Toulouse France.

c. Laboratoire des IMRCP, Université de Toulouse, CNRS UMR 5623, Université Paul Sabatier, 118 route de Narbonne, 31062 Toulouse Cedex 9, France.

KEYWORDS. vitrimers, epoxy, resin transfer moulding, TTT diagram

ABSTRACT: Over the last few years, scientists have developed new ways to overcome the recycling issues of conventional thermosets with the introduction of associative covalent adaptable networks (i.e. vitrimers) in polymer materials. Even though various end-use vitrimers were already reported, just few of them targeted high performance industrial applications. Herein, we develop a promising high-performance epoxy vitrimer based on a commercially available resin widely used in aeronautics with the highest glass transition temperature (Tg) of 233°C ever reported for a vitrimer. A complete study of its physico-chemical properties and cure kinetics was conducted enabling the construction of the first time-temperature-transformation (TTT) diagram reported in the literature. This diagram allows a full determination of the processing and curing parameters leading to the manufacturing of vitrimers samples by Resin Transfer Moulding (RTM) process. The reshapability and limits therefrom of this high Tg vitrimer was evaluated by three successful thermoforming cycles without degradation.

1. Introduction

Aeronautics uses more and more thermosets for high performance applications (e.g. structural parts such as fuselage or wings) owing to their exceptional durability and structural integrity.[1] They are also commonly used in many other areas such as transportation or energy (e.g. wind turbines). In many applications, there are usually combined with reinforcements such as carbon or glass fibres (fibre-reinforced polymer composites (FRPC)) which exhibit very competitive strength/weight ratio that can outperform metal materials in many settings. Current recycling processes use thermolysis,[2,3] solvolysis[4,5] or other methods[6,7] to degrade the polymer matrix from a composite part, so that the reinforcements can be reclaimed and reused, but mostly with altered mechanical properties.[8] Therefore, these fibres cannot be recycled several times and used for the same applications as they were initially intended for.[5,9,10]

In the last few years, the scientific community has developed new approaches to overcome the difficulty of recycling thermosets matrices by either introducing cleavable bonds into the polymer matrix (but with often detrimental loss of properties) or by replacing the permanent bonds with dynamic analogues. The later strategy involving dynamic bonds endows these polymer materials with new properties such as reprocessability, healability and recyclability. Among the large research thematic dealing with dynamic materials, vitrimers appear as a promising alternative gathering the advantages of thermosets with good mechanical characteristics and viscous flow at high temperature. Vitrimers properties are induced by an associative exchange mechanism in the polymer network which maintain the cross-link density constant during thermal activation with an unchanged number of chemical bonds through the reprocessing procedure.[11] This confers to vitrimers similar characteristics to those of vitreous glass at high temperature (*i.e.* Arrhenius dependence of viscosity with temperature) facilitating healing and reprocessing without the need of precise temperature control.

Since then, a strong enthusiasm has emerged from the composite community to implement the recently developed dynamic chemistries for industrially relevant composites parts. For a more exhaustive report on vitrimers composites, the reader is directed to our recent review[12] and some other related reports.[13,14] Among the many different chemistries implemented or purposely developed by

chemists[11,15–17] for vitrimers, only few of them were used in the context of composites: transesterification,[18,19] transamination of vinylogous urethanes,[20,21] disulfide exchanges,[22,23] and imine exchanges,[24,25] to name the most popular ones. This poor diversity is strongly connected to the limited large-scale commercial availability of dynamic chemical precursors preventing the use of sophisticated chemical platforms. Besides simple availability considerations, their implementation in practical industrial applications is not straightforward, especially for aeronautics where the qualification process is very strict and lengthy. For some aeronautical applications, a high glass transition temperature (>200 °C) is one of the most important characteristics to consider. However, only few recent reports fulfil this criterion[26,27] with most of the reports exhibiting T_g below 170 °C.[28–30] Ruiz de Luzuriaga and co-workers recently developed a high T_g epoxy vitrimer based on commercial resins TGMDA (MY21) and DGBF (PY306) and compared its properties to those of aerospace-certified resin Hexcel HexFlow® RTM6 which is widely used in industry for many decades and especially designed for resin transfer moulding (RTM) process. [26,27] However, the resulting resin afforded a glass transition of 176 °C still well below the T_g of 220 °C of RTM6-based thermoset benchmark. In addition, the optimisation of the composite manufacturing process RTM was not investigated. Zhang and co-workers used one of the RTM constituents (tetraglycidyl methylene dianiline, TGDDM) which they cross-linked by epoxy/anhydride reactions affording materials with high mechanical performance and high T_g (>200 °C). [26,27] However, the modification of the crosslinking strategy from epoxy/amine towards epoxy/anhydride considerably modified the crosslinking procedure and network composition with the formation of hydrolytically sensitive ester bonds. A full network degradation was achieved in pure water without addition of catalyst. Although being an interesting property for certain applications, it becomes crippling in the context of aeronautical specifications. From a composite manufacturing process point of view, although a few papers reported vitrimer composites produced by RTM,[26,31–33] none of them studied completely the crosslinking kinetics and reactivity with a time-temperature-transformation (TTT) diagram and the optimisation of the process parameters and curing cycles. TTT diagrams[34,35] were developed in the mid 80's and widely used for thermosets, but were never reported for vitrimer materials, to the best of our knowledge.

Therein we report a high-performance epoxy vitrimer based on the commercial epoxy resin RTM6-2[36] widely used in aeronautics and with the highest glass transition of 233 °C ever reported for vitrimers. A comprehensive cure kinetics study was conducted enabling the construction of the first time-temperature-transformation (TTT) diagram for a vitrimer. This TTT diagram enabled the production of vitrimer plates by resin transfer moulding (RTM) process, and their reprocessability /reshapability properties and limitations were especially investigated.

2. Experimental

2.1. Materials

HexFlow® RTM6-2 Part A (4,4'-Methylenebis[N,N-bis(2,3-epoxypropyl)aniline]) and Part B (4,4'-Methylenebis(2,6-diethylaniline) 60-100%, 4,4'-Methylenebis(2-isopropyl-6-methylaniline) 30-60%) was purchased from Hexcel. 4-aminophenyl disulfide (4-AFD) was purchased from Molekula group.

2.2. Characterizations

Densities were obtained using the Density Determination Kit Sartorius YDK03 at room temperature. The reported results are averages of three measurements.

Soxhlet experiments were conducted using chloroform at reflux temperature for 24h. After Soxhlet experiments, the samples were carefully removed and dried in a vacuum oven at 120°C during 24h to remove the solvent remaining. Then, the soluble fraction was calculated according to equation [1].

$$\text{Soluble fraction (\%)} = \frac{m_{\text{initial}} - m_{dry}}{m_{initial}} \text{ x } 100\% \qquad [1]$$

Differential scanning calorimetry (DSC) analyses were performed with a DSC 25 TA instruments under nitrogen atmosphere at different isotherms and/or ramps in standard mode. The modulated mode was also used with the following parameters: ramp 2°C/min, period 120s and amplitude ± 1 °C.

Thermogravimetric analyses (TGA) were performed with a TG 209 F3 Tarsus Netzsch under air at a heating rate of 10°C/min from 30°C to 900°C.

Rheological analyses were performed with a rheometer MCR 302 Anton Paar. Oscillatory measurements using parallel plates of 25 mm diameter with a gap of 0.5 mm, an angular velocity of 10 rad/s and a strain of 4% were typically used (in the linearity zone).

Dynamic Mechanical Analyses (DMA) were performed with a DMA+ 100 Metravib under air at a heating rate of 3°C from 25°C to 280°C. Measurements were performed in tensile mode with a static strength of 2N, a frequency of 1 Hz, a displacement of 15 µm (in the linear viscoelastic region) on rectangular samples measuring 40 x 6.00 x 1.20 mm. The reported results are averages of three measurements.

3 point flexural tests were performed with an INSTRON 4466 and an adapted 3 point flexural bench in accordance with the ISO 14125 standard, 3 samples per system.

Stress relaxation experiments were performed with a hybrid rheometer HR20 TA Instruments under air at different isotherms. After reaching the requested temperature, a waiting time of 15 minutes was set for the system to reach the equilibrium before applying the strain. Measurements were performed in 3 point flexural mode with a strain of 0.5% on rectangular samples measuring 40 x 6.00 x 1.10 mm.

2.3. Synthesis of RTM6 vitrimer

The RTM6-2 reference epoxy network was prepared following the recommendations of Hexcel: the weight ratio between the RTM6-2 part A and part B was fixed at 100 : 68.1. For the RTM6-V network, the weight ratio of RTM6-2 part A and 4-AFD was fixed at 100 : 54.5. For both systems, the epoxy resin and the hardener were mixed and stirred at 80°C for 30 minutes to obtain a homogeneous mixture.

2.4. Manufacturing of RTM6 vitrimer by Resin Transfer Moulding

After obtaining the mixture, two manufacturing processes were used to produce plates: moulding and RTM. For the conventional moulding, the mixture under stirring was degassed at 70°C for 20 min in a vacuum chamber and poured in a mould, then cured at 180°C during 90 minutes for the RTM6-2; and 170°C during 90 minutes for the RTM6-V. The dimensions of the plates obtained were 150 x 40 x 2 mm.

The RTM manufacturing unit is comprised of an injection unit Isojet and a heat press Enerpac to maintain the mould closed. Furthermore, the mould, made of stainless steel with different gaps to control the final plate's thickness contains 1 injection port and 1 vacuum port on opposite sides (Figure S1). The final plates obtained measured 300 x 300 x 4 mm.

3. Results and discussion

One of the objectives of this work is the construction of a TTT diagram which is of paramount importance to set the parameters of industrial manufacturing processes such as RTM. To do so, the chemical structure of the RTM6-2 part A (epoxy resin) and part B (permanent hardener) was studied in order to select a dynamic hardener compatible with the RTM6-2 part A chemistry and commercially available. The use of aromatic amine for the dynamic hardener was an important prerequisite in order to reach a similar reactivity/cure kinetics to the one obtained with RTM6. Hence, 4-AFD (4-aminophenyl disulfide) was selected as dynamic hardener and its reactivity with RTM6 epoxy resin was deeply investigated and strictly compared to the permanent hardener reference (RTM6-2 part B), Figure 1. The dynamic properties are introduced through the disulfide linkage embedded within the dynamic hardener which undergoes both associative and dissociative mechanisms at high temperature through a radical-mediated mechanism.[37,38] The general synthetic routes to obtain both types of networks are described in Figure 1.[39] Because the difference of structure may lead to non-negligible differences in reactivity and change in viscosity, this aspect is deeply investigated in the following sub-section.

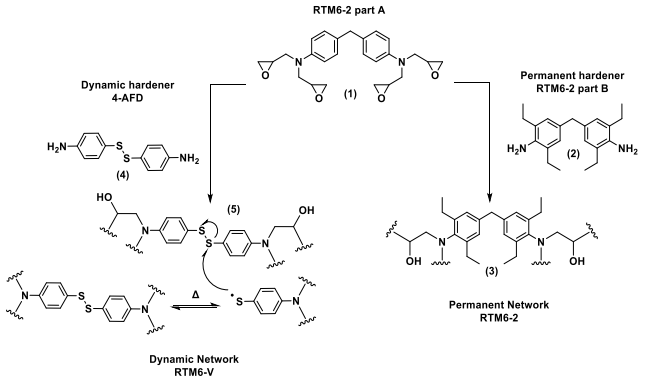

Figure 1. Reactions occurring between **(1)** RTM6-2 part A (epoxy resin) and **(2)** RTM6-2 part B (permanent hardener) to obtain **(3)** reference epoxy thermoset RTM6-2. The reaction between **(1)** and **(4)** 4-AFD gives **(5)** RTM6-V network.

3.1. Crosslinking kinetics and TTT diagram

To build and determine the cure kinetics model and its parameters, the crosslinking kinetics of the RTM6 vitrimer (RTM6-V) and RTM6-2 permanent analogue were evaluated by rheological experiments and DSC analyses. First, the complex viscosity η* (at 10 rad.s-1) was determined at typical processing temperature since a low complex viscosity (< 1000 mPa.s) is mandatory for RTM process. For both mixtures, a complex viscosity lower than 1000 mPa.s was obtained at temperatures from 110°C up to 160°C for RTM6-V and RTM6-2 (Figure 2).

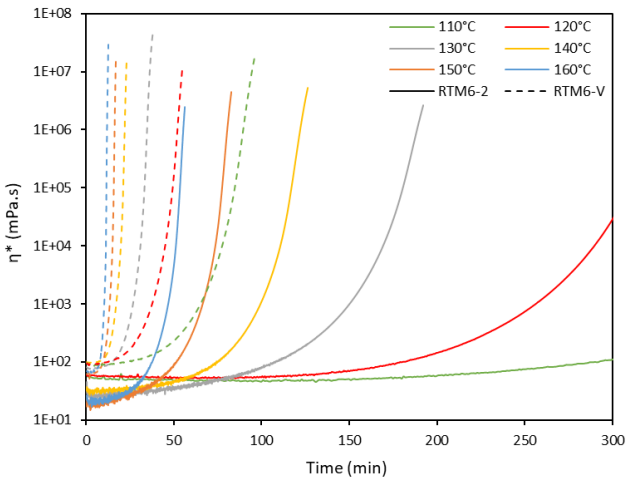

Figure 2. Complex viscosities as a function of time for different isotherms (130°C to 160°C) for the RTM6-V compared to the RTM6-2.

A faster reactivity is clearly visible (Figure 2) for RTM6-V with a complex viscosity of 10^3 mPa.s reached after 27 min compared to 150 min for the RTM6-2 permanent analogue (130 °C). In addition to viscosity, the gel times were also determined in this temperature range[40] (Figures S2, S3 and Table 1). A similar trend was observed with a significant decrease of gel times by a factor of 5 for the vitrimer. Owing to the higher reactivity of 4-AFD *vs* RTM6-2 part B, the curing procedure of RTM6-V is faster than typical RTM6-2 for comparable temperatures or could be purposely conducted at lower temperatures to reduce the overall manufacturing process costs.

Table 1. Gel times in minutes for different isotherms for RTM6-2 and RTM6-V.

Curing isotherm	130°C	140°C	150°C	160°C
RTM6-2	193.3	122.4	80.0	54.1
RTM6-V	34.5	21.5	15	10.5

Different DSC experiments were also conducted. Firstly, isothermal DSC experiments were performed at different temperatures for RTM6-V and RTM6-2. Then, the changes in the degree of conversion as a function of time were calculated using equation [2]:

$$\alpha = \frac{\int_0^t \frac{dH}{dt} dt}{\Delta H_T} \quad [2]$$

With α the degree of conversion, the integration from 0 to t represents the enthalpy of reaction at a specific time and ΔH_T the total reaction enthalpy. Secondly, isothermal DSC curves were used to identify the parameters of a phenomenological Kamal-Sourour model[41] defined by equation [3]:

$$\frac{d\alpha}{dt} = (k_1 + k_2\alpha^m)(1-\alpha)^n \quad [3]$$

With $d\alpha/dt$ the reaction rate, k_1 and k_2 the reaction rate constants following an Arrhenius-type dependence on temperature [4], α the fractional conversion and m and n the reaction orders. This law has been used several times in the literature to model the polymerisation of epoxy resins.[42–45]

$$k_i(T) = A_i e^{\frac{-E_i}{RT}} \quad i = 1;2 \quad [4]$$

With A_i the pre-exponential factor, E_i the activation energy of the system following an Arrhenius law, R the universal gas constant and T the curing temperature. The parameters of the Kamal-Sourour model were identified on the isothermal curves using a Nelder-Mead simplex direct search.[46,47] The objective function of this unconstrained multivariable optimization is the normalized difference between the numerical solution and the experimental data. The fitting line equation (Figures S4 and S5) of the optimized set of parameters were then obtained to determine the activation energies and the pre-exponential factor of the rate constants. Regarding the reaction order m, it does not follow any significant temperature trend and is rather constant, and this whatever the temperature of the DSC isothermal scans. Therefore, the mean value was taken to obtain a global modelling of the system. However, this is not the case for the reaction order n, which linearly increases with temperature. The information on parameters of the global Kamal-Sourour model obtained for RTM6-V is gathered in Table 2 compared to the standard RTM6-2 system.

Table 2. Parameters of the global Kamal-Sourour model for RTM6-V compared to RTM6-2.

	RTM6-2	RTM6-V
A_1 (s^{-1})	$6.99.10^4$	$5.96.10^5$
A_2 (s^{-1})	$1.12.10^5$	$3.47.10^4$
E_1 ($kJ.mol^{-1}$)	73.93	73.75
E_2 ($kJ.mol^{-1}$)	63.81	51.88
m	1.41	1.76
n	0,0145*T-1,21	0.0083*T+0.26

Afterwards, the experimental data were compared to the identified Kamal-Sourour model for RTM6-V (Figure 3) and RTM6-2 (Figure S6) as a comparison.

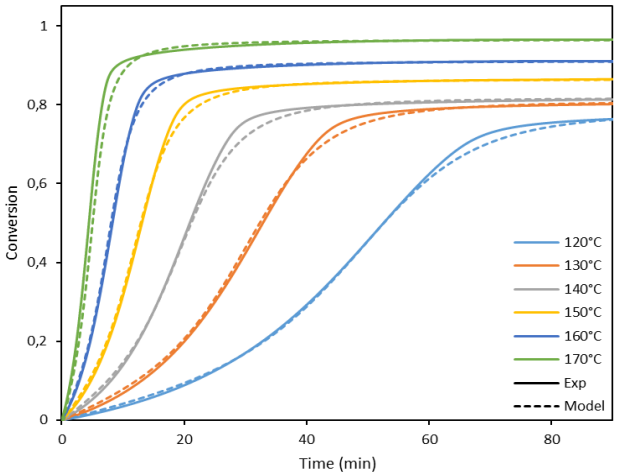

Figure 3. Conversion curves as a function of time during the curing at different isotherms for RTM6-V.

Even though this model is based on isothermal curing, it could be extended and applied to dynamic curing with different heating ramps from 1°C/min to 10°C/min with satisfactory fitting for both networks (Figures S7 and S8). It is important to note that the pre-exponential factor A_1 and A_2 are strikingly different for RTM6-2 and RTM6-V. A stronger contribution of A_1 compared to A_2 is observed for RTM6-V implying a strong dependency towards initiated and catalysed reaction from H-donor moIecuIes with no or low influence of internally catalysed reactions from generated hydroxyl groups. In contrast, RTM6-2 shows a balanced contribution of both reactions. This difference could explain the higher reactivity of 4-AFD compared to RTM6-2 part B especially at low conversion.

The correlation between the gel times (Table 1) obtained at different isotherms with oscillatory rheological and isothermal DSC experiments (Figure 3) led to the determination of the specific degree of conversion to a change from a liquid to a gel state of the resins, and considered independent of temperature (Table 3). α_{gel} values obtained lay within the usually found α_{gel} range for epoxy thermosets.[48]

Table 3. Specific degrees of cure α_{gel} obtained at different curing isotherms for RTM6-V compared to RTM6-2.

Curing isotherm	120 °C	130 °C	140 °C	150 °C	160 °C	170 °C	180 °C	$\overline{\alpha_{gel}}$
$\alpha_{gel,RTM6-2}$	-	-	0.71	-	0.73	0.72	0.78	**0.74 ± 0.03**
$\alpha_{gel,vitrimer}$	0.50	0.53	0.53	0.60	0.66	-	-	**0.56 ± 0.06**

Furthermore, T_g can be linked to the degree of conversion using the Di Benedetto's equation[49] [5]:

$$T_g = T_{g0} + (T_{g\infty} - T_{g0}).\frac{\lambda\alpha}{1-(1-\lambda)\alpha} \quad [5]$$

Where T_{g0} and $T_{g\infty}$ are respectively the glass transition temperatures for the uncrosslinked ($\alpha = 0$) and fully crosslinked ($\alpha = 1$) polymer, and λ a structure-dependent parameter. Theoretically λ is equal to $\Delta C_{p\infty}/\Delta C_{p0}$, where $\Delta C_{p\infty}$ and ΔC_{p0} are the differences in heat capacity through the glass transition for a fully cured and uncured systems, respectively. Isothermal DSC experiments were conducted and interrupted at different times in order to determine T_g and the residual heat of reaction ΔH_{res} (i.e. conversion calculated with [6]) for each experiment.

$$\alpha = 1 - \frac{\Delta H_{res}}{\Delta H_T} \qquad [6]$$

λ was determined, thus giving access to the evolution of T_g as a function of the degree of conversion for both networks (thermoset and vitrimer),Figure 4.

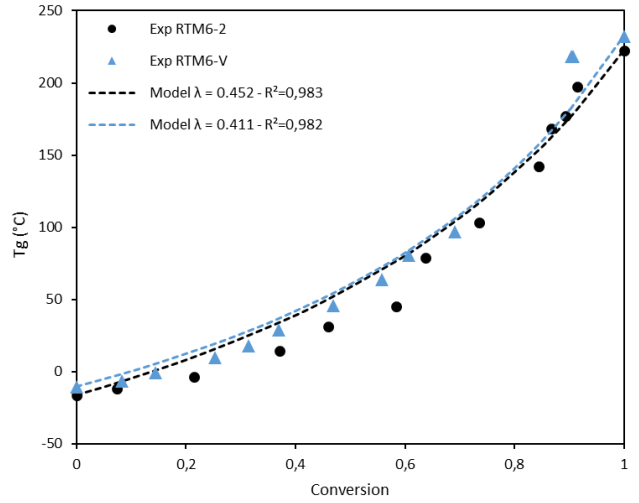

Figure 4. Experimental and Di Benedetto's model curves for RTM6-2 and RTM6-V.

Finally, the results were combined into so-called TTT (Time, Temperature, Transformation) diagrams widely used for thermoset polymers and especially for epoxy resins.[34] The TTT diagrams of RTM6-2 as a reference and RTM6-V are presented Figure 5.

TTT diagrams are important as they illustrate in one graph the critical temperatures and material state modifications that are taking place during crosslinking (gelation, vitrification, complete crosslinking and degradation). This information can then be used to define the parameters of the manufacturing process, but also to determine an optimized curing cycle.

The conventional TTT diagram is usually comprised of 3 types of curves: vitrification, gelation and isoconversional curves. The vitrification and gelation curves represent the border between the different states of the thermoset/vitrimer resin during a curing cycle. More precisely, the vitrification curve is reached when T_g is equal to the isothermal curing temperature (T_{cure}). Isoconversional curves (herein from $\alpha = 0.1$ to $\alpha = 0.99$) indicate the increase of the conversion degree during the curing cycle, but can also be very useful to set a limit of temperature/time for the manufacturing processes. Herein, the isoconversional curves were plotted before reaching vitrification. Indeed, after this point the model used could not be extrapolated to the glassy domain since the cure kinetics becomes very slow and the reaction is diffusion-controlled. Furthermore, the TTT diagram includes the glass transition temperature of the uncured (T_{g0}) and fully cured ($T_{g\infty}$) resin, but also $T_{g,gel}$. $T_{g,gel}$ is defined as the intersection point between gelation and vitrification curves and was calculated using the Di Benedetto's equation [4] with $\alpha = \alpha_{gel}$.

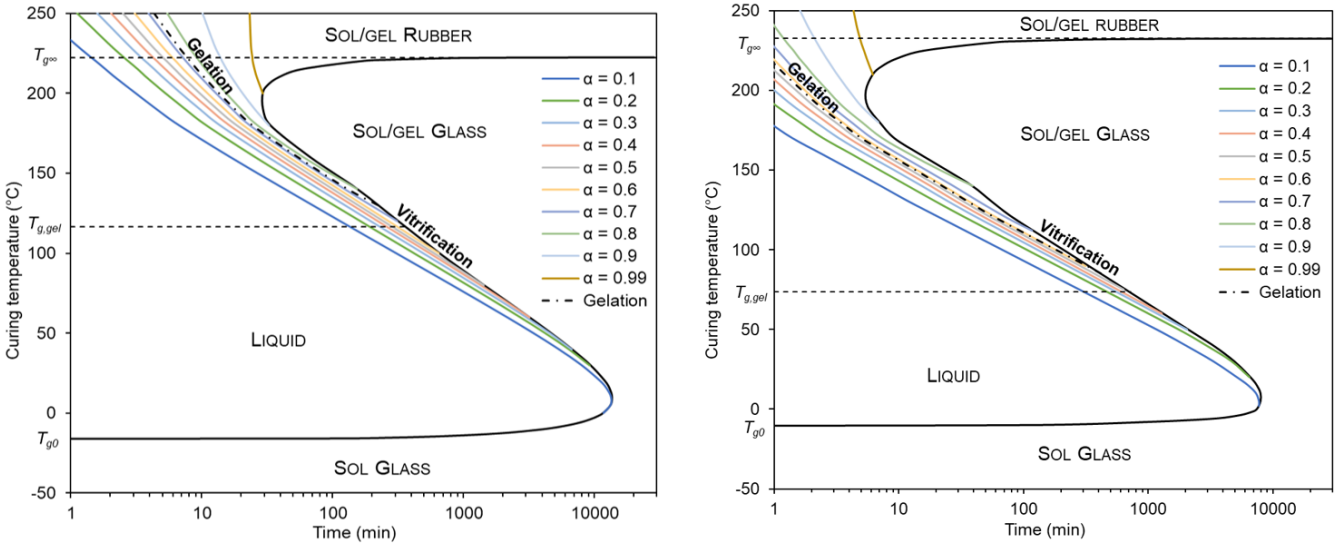

Figure 5. TTT diagram of RTM6-2 (**left**) and RTM6-V (**right**).

As noticed before, these diagrams confirm the faster crosslinking kinetics of RTM6-V compared to RTM6-2 reference network. For instance, at a curing temperature of 180°C for RTM6-2 it would take around 31 minutes to reach a curing degree of at least 0.9 while it would only take 8 minutes for the RTM6-V. In addition to the sought reprocessing properties, this could have a real positive impact on the manufacturing cost, directly linked to temperature and curing time to produce polymer and composite parts enabling energy savings.

As previously mentioned, a viscosity below 1000 mPa.s is necessary for injection. In that regard, manufacturing systems must be heated to reach sufficiently low viscosity, but this increase in temperature initiates polymerisation which results in shorter time frame to manufacture parts. Therefore, a compromise should be found between the viscosity needed to produce a specific part and the time needed for the manufacturing process before curing. Preliminary studies and TTT diagrams enabled the resin injection pressure and curing temperature paths to be determined (Figure 6).

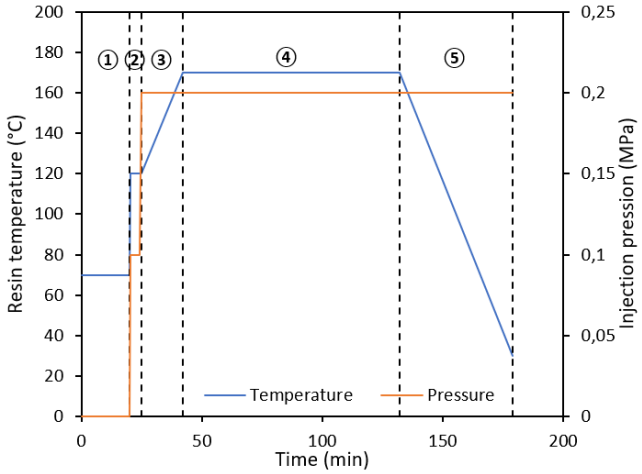

Figure 6. Injection and curing profile of RTM6-V. 1 Degassing in the vacuum chamber at 70°C and 15 mBar during 20 minutes. 2 Filling in the mould (120°C) at 0.1 MPa (1 bar) + post filling at 0.2 MPa. 3 Heating ramp from 120°C to 170°C at 3°C/min. 4 Isotherm curing at 170°C during 90 minutes. 5 Cooling ramp from 170°C to 30°C at 3°C/min.

A temperature of 70°C in the RTM injection pot (Figure 6.1) was thus selected for RTM6-V and RTM-2 analogue giving more than 3 hours and more than 15 hours for the outgassing and injection process, respectively. During the injection step, the resin temperature is gradually increased to 120°C (Figure 6.2) thanks to a heating jacket around the injection tube (Figure S9). This elevation of temperature was necessary to decrease the resin viscosity and hence facilitating the resin injection in the mould cavity. After the mould filling, a post filling at a higher pressure was performed to avoid the presence of porosities. Finally, a heating ramp from 120°C to 170°C (RTM6-V) and 180°C (RTM6-2) at 3°C/min was applied (Figure 6.3) and then a curing isotherm during 90 minutes (Figure 6.4). Afterwards, the mould was cooled down at 3°C/min to ambient temperature, and the plates were removed from the mould. Two plates for each system were produced with dimensions of 300 x 300 x 4 mm.

3.2. Physico-chemical and mechanical properties

Different analyses were conducted to characterize the physico-chemical properties of both networks (Table 4). Samples were taken on plates manufactured by conventional moulding and RTM, and identical properties were obtained. From now, all results presented for cured samples come from plates manufactured by RTM following the process parameters presented in section 2.1. In addition, the aromatic structure of the 4-AFD is relatively close to the structure of the permanent hardener, thus a high T_g (>200°C) is in principle expected. However, some differences may have a significant impact on the final material properties. For instance, the RTM6-2 hardener (Figure 1.(2)) consists of β-diethyl substituents which are not present in the 4-AFD (Figure 1.(4)). This means that RTM6-2 network should exhibit higher free volume than RTM6-V analogue with possible impact on network density and T_g. Therefore, the density was verified for both materials on three samples and the results are listed Table 4.

As theoretically expected, a higher density was obtained for the RTM6-V with an obtained value of 1.267 compared to 1.145 for the thermoset reference. The density of the reference network corresponds to the one given by the technical datasheet of RTM6 resin manufacturer[36] and the increase of density with the use of 4-AFD was also noticed by Ruiz de Luzuriaga et al.[26] The 10% increase in the density of RTM6-V system can be somewhat penalizing for aeronautical applications where engineers always aim to lighten parts and structures, but this could be compensated with all the benefits of vitrimers compared to conventional thermosets.

The thermal stability of RTM6-V is a key parameter for processing and reprocessing the vitrimer. TGA measurements of the onset degradation associated to a 5% mass loss is observed at 291.4°C for the vitrimer while the reference is stable up to 319.9°C (Figures S12 and S13). This decrease of thermal stability for RTM6-V is likely due to the presence of the disulfide bonds as described in the litterature.[22]

Table 4. Physico-chemical properties of RTM6-2 and RTM6-V obtained by: a. Soxhlet; b. DSC; c. DMA; d. TGA. E' values were taken at 30°C.

	Density	Gel content (%)$_a$	Tg_0 [°C]$_b$	Enthalpy [J/g]$_b$	Exothermic peak [°C]$_b$	Tg_∞ [°C]$_b$	T_α [°C]$_c$	E' [GPa]$_c$	T_d [°C]$_d$
RTM6-2	1.145 ± 0.003	0.15	-16.7	496.1	242.0	222.5	233.6 ± 2.0	2.58 ± 0.17	319.9
RTM6-V	1.267 ± 0.001	0.85	-10.6	589.0	200.5	232.5	243.1 ± 1.0	2.71 ± 0.12	291.4

From DSC measurements (Figures S10 and S11), comparable glass transition temperatures were obtained for both networks but with an enthalpy of crosslinking largely increased for RTM6-V (+93 J/g). In addition, the exothermic peak has been lowered by more than 40°C for the vitrimer showing again that cross-linking reactions occurred at lower temperatures.

Dynamic mechanical analysis (DMA) was also carried out on cured resin samples (Figure 7) to study the influence of the dynamic hardener on the storage modulus and the alpha temperature (T_α). The α peak is the main mechanical relaxation and corresponds to the mechanical manifestation of the glass transition with T_α being the corresponding temperature at the α peak.

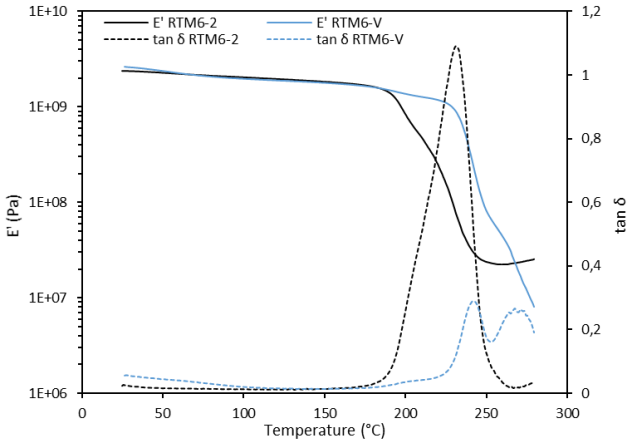

Figure 7. Dynamic mechanical analysis (DMA) for a 3°C/min ramp from T_{amb} to 280°C for RTM6-2 and RTM6-V.

The storage modulus E' of both systems was identical and the T_α slightly increased for RTM6-V meaning that the use of 4-AFD as hardener did not affect these properties. The width of the T_α peak is also similar implying comparable homogeneity of the networks. In contrast, the decrease of T_α height suggests a more elastic network for RTM6-V than RTM6-2.

Furthermore, 3 point flexural test were chosen to characterise the mechanical strength of RTM6-V compared to RTM6-2 reference network (Figure 8).

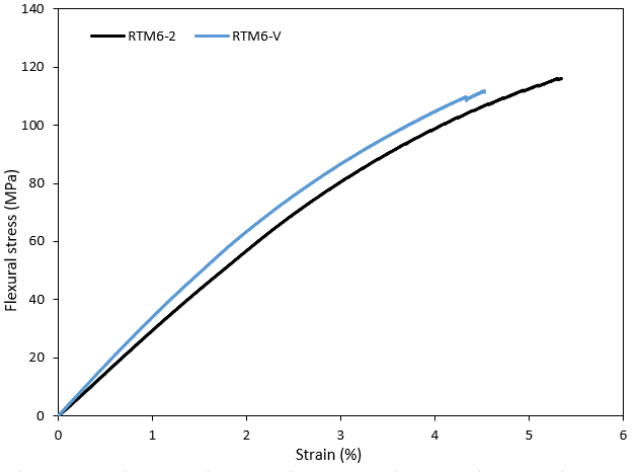

Figure 8. 3 point flexural stress (MPa) as a function of strain (%) for RTM6-V compared to RTM6-2.

Indeed, this test reflects the ability of the samples tested to withstand compressive, tensile and shear constraints and is best suited for the reprocessing by thermoforming of RTM6-V described in the next section. The maximal flexural stress (σ_{max}), strain (ε_{max}) and flexural modulus (E_f) are reported Table 5.

Table 5. Mechanical properties obtained by 3 point flexural tests for RTM6-V compared to RTM6-2.

	σ_{max} (MPa)	ε_{max} (%)	E_f (GPa)
RTM6-2	118.7 ± 4.6	5.42 ± 0.51	2.94 ± 0.03
RTM6-V	110.4 ± 6.6	4.57 ± 0.66	3.34 ± 0.17

The maximal flexural stress obtained for both networks is identical and corresponds to high performance polymers. For RTM6-V, a lower strain and a higher flexural modulus indicates a slightly stiffer network; which should not have a significant influence on the mechanical properties of composites produced using this matrix.

3.3. Reprocessing of RTM6 vitrimer

The main issue with such high T_g vitrimers is the reprocessing temperature frame. Indeed, to activate the dynamic bonds and have enough polymer-chain mobility, the reprocessing temperature needs to be higher than T_g and lower than the degradation temperature T_d. If T_g is too close to T_d, it might be not possible to fully reprocess the material without degrading it.

Following the TTT diagram of the aforementioned RTM6-V, unreinforced RTM6-V plates produced by RTM were tested. Stress-relaxation experiments were conducted at an isothermal temperature of 245°C to highlight the reprocessability of the vitrimer (Figure S14). This temperature was chosen above T_g and below T_d to avoid as much as possible any degradation of the materials. In a very short time, RTM6-V could fully relax the stress giving a relaxation time τ* of around 50 seconds.

After validating the stress relaxation of RTM6-V, its reprocessability was investigated. Generally, two main different ways to reprocess vitrimers are studied: mechanical grinding followed by reprocessing in a mould to obtain a new plate, or reshaping by thermoforming to obtain the same plate reshaped.

Firstly, RTM6-V plates were ground into flakes, poured into a stainless-steel mould inserted into a hot press. The temperature, time and pressure are the parameters to optimize in order to obtain the best reprocessed plates. Despite different settings studied, it could not be possible to reprocess the RTM6-V plate without starting to degrade it due to its very narrow reprocessing temperature window (Figure S15). Indeed, such reprocessing would need a longer time or a higher temperature to obtain acceptable reprocessed plates, which is here intrinsically not possible without degradation.

Nevertheless, as RTM6-V is targeted to be used to manufacture composites materials using long carbon fibre reinforcements, reprocessing after grinding is not really

relevant as it will significantly impair mechanical properties. Effectively, changing the shape of a composite part from a flat plate into an L-shape stiffener for reusing it for instance is one capability of vitrimer matrices. Another interesting property lies in the possibility of "self-healing" delamination and cracks between the plies of a vitrimer matrix composite stemming from a low energy impact.

Therefore, thermoforming experiments were conducted on RTM6-V plates in 3 point bending at 245°C (Figure 9). Every thermoforming cycle was comprised of: (i) inserting the vitrimer flat sample into the oven at 245°C, (ii) enabling the sample to stabilise at 245°C for 2 minutes, (iii) applying a vertical displacement of 6 mm at a rate of 0.1 mm/s, (iv) maintaining this 6 mm displacement for 1 minute enabling thus internal stresses to be relaxed, (v) the samples are taken out from the oven and freely cool down to room temperature.

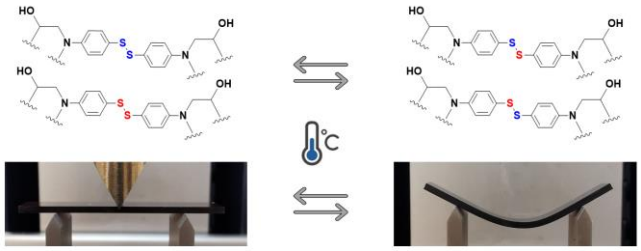

Figure 9. Reshaping of an RTM6-V sample (bottom) in a few seconds thanks to its dynamic exchanges (top).

The L-shape samples obtained by 3-point bending are taken back to their initial flat shape by putting them back in the oven at 245°C and mechanically cancelling their deflection. This corresponds to a whole duration of 8 minutes of thermoforming (R1). This thermoforming process was applied up to 3 times to the same sample in order to assess its reforming ability several times in a row, respectively R2 and R3. No visual degradation was observed during the thermoforming process, and this was confirmed with ATR-FTIR curves obtained with R0 (no reshaping), R1, R2 and R3 (Figures S17 and S18) even though isothermal TGA at 245°C revealed a loss of mass of 2.5%, 3.3% and 4.0% for R1, R2 and R3, respectively (Figure S16). The aforementioned samples were stored at room temperature during 10 months and a drying procedure in an oven highlighted a water uptake of almost 1 wt%, meaning the mass losses recorded R1 to R3 cycles must be corrected to give 1.5%, 2.3% and 3% losses linked to degradation by-products other than water. FTIR measurements were conducted on both surface (Figure S16) and core (Figure S17) of the samples, showing for the surface analysis the appearance of an oxidation peak at 1660 cm^{-1}, which was not detected in their core. FTIR results presumably mean that this residual mass loss was not originated from the main functional bonds of the vitrimer network.

DMA experiments were also performed on the reshaped samples to ensure no degradation of the mechanical properties (Figure 10). Even after 3 thermoforming cycles (R3), the samples conserved their initial storage modulus and T_α.

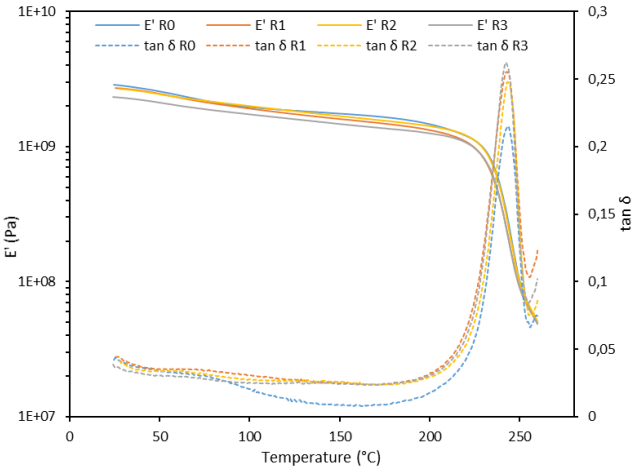

Figure 10. DMA for a 3°C/min ramp from T_{amb} to 260°C of RTM6-V samples reprocessed x times (noted Rx).

Thus, the thermoforming of unreinforced RTM6-V was successfully conducted up to 3 times with no degradation noticed by FTIR and DMA. This result suggests that despite the tight temperature window, the reshaping of this high T_g vitrimer was still possible opening various opportunities for correcting/repairing industrial parts.

3. Conclusions

In summary, we have demonstrated the possibility to obtain a high-performance epoxy vitrimer based on the commercial epoxy resin RTM6-2 widely used in aeronautics and with the highest glass transition of 233 °C ever reported for vitrimers. A complete study of its physico-chemical properties and a comprehensive crosslinking kinetics study was conducted enabling the construction of the first time-temperature-transformation diagram reported for a vitrimer. The replacement of the permanent hardener by a dynamic analogue did not considerably modify the curing behaviour nor the physico-chemical/mechanical properties of the resulting materials, although a slightly higher reactivity was evidenced. The TTT diagram enabled the production of vitrimers samples by RTM process with a full control of the processing and curing parameters. Due to its very narrow reprocessing window, the reprocessability by mechanical grinding presented severe limitations. Nevertheless, the reshapability was highlighted by the successful thermoforming of RTM6-V samples up to 3 reshaping cycles, which could answer the needs of the composite industry concerning the deformation or damages of laminated composite parts; and therefore, drastically reduce the number of rejected parts. Further investigations remain to be done on high T_g (~230°C) carbon fibre reinforced RTM6-V composites and their thermoforming ability.

ASSOCIATED CONTENT

"The supporting information is available free of charge via the Internet at http://pubs.acs.org."
Rheological experiments, DSC and TGA thermograms, FTIR, and images of reprocessed materials.

AUTHOR INFORMATION

Corresponding Author

* philippe.olivier@iut-tlse3.fr
* marc.guerre@cnrs.fr

Author Contributions

The manuscript was written through contributions of all authors. All authors have given approval to the final version of the manuscript.

Notes

The authors declare no competing financial interest.

ACKNOWLEDGMENT

The authors would like to thank the technological research institute Saint Exupéry for financial support.

REFERENCES

(1) Ratna, D. Chapter 4 - Thermoset Composites. In *Recent Advances and Applications of Thermoset Resins (Second Edition)*; Ratna, D., Ed.; Elsevier, 2022; pp 371–418. https://doi.org/10.1016/B978-0-323-85664-5.00001-6.

(2) Boulanghien, M.; R'Mili, M.; Bernhart, G.; Berthet, F.; Soudais, Y. Fibre Characterisation of Steam Thermal Process Recycled Carbon Fibre/Epoxy Composites. In *ICCM 19 -19th International Conference on Composite Materials*; Montreal, Canada, 2013; p p.9087-9094.

(3) Boulanghien, M.; R'Mili, M.; Bernhart, G.; Berthet, F.; Soudais, Y. Mechanical Characterization of Carbon Fibres Recycled by Steam Thermolysis: A Statistical Approach. *Advances in Materials Science and Engineering* **2018**, *2018*, e8630232. https://doi.org/10.1155/2018/8630232.

(4) Prinçaud, M.; Aymonier, C.; Loppinet-Serani, A.; Perry, N.; Sonnemann, G. Environmental Feasibility of the Recycling of Carbon Fibers from CFRPs by Solvolysis Using Supercritical Water. *ACS Sustainable Chem. Eng.* **2014**, *2* (6), 1498–1502. https://doi.org/10.1021/sc500174m.

(5) Oliveux, G.; Bailleul, J.-L.; Gillet, A.; Mantaux, O.; Leeke, G. A. Recovery and Reuse of Discontinuous Carbon Fibres by Solvolysis: Realignment and Properties of Remanufactured Materials. *Composites Science and Technology* **2017**, *139*, 99–108. https://doi.org/10.1016/j.compscitech.2016.11.001.

(6) Nunes, A. O. Carbon fiber reinforced composites : recovery of carbon fiber by steam-thermolysis, optimization of the process. phdthesis, Ecole des Mines d'Albi-Carmaux, 2015. https://theses.hal.science/tel-02003515 (accessed 2023-01-18).

(7) Jlassi, S.; Berthet, F.; Bernhart, G. Investigation of Mechanical Properties of Nonwoven Second Generation Composite Material Elaborated through a Mixture of Carbon Fibers and Filament Lengths. In *ECCM18 - 18th European Conference on Composite Materials*; 2018; Vol. hal-01862432.

(8) Rani, M.; Choudhary, P.; Krishnan, V.; Zafar, S. A Review on Recycling and Reuse Methods for Carbon Fiber/Glass Fiber Composites Waste from Wind Turbine Blades. *Composites Part B: Engineering* **2021**, *215*, 108768. https://doi.org/10.1016/j.compositesb.2021.108768.

(9) Verma, S.; Balasubramaniam, B.; Gupta, R. K. Recycling, Reclamation and Re-Manufacturing of Carbon Fibres. *Current Opinion in Green and Sustainable Chemistry* **2018**, *13*, 86–90. https://doi.org/10.1016/j.cogsc.2018.05.011.

(10) Zhang, J.; Chevali, V. S.; Wang, H.; Wang, C.-H. Current Status of Carbon Fibre and Carbon Fibre Composites Recycling. *Composites Part B: Engineering* **2020**, *193*, 108053. https://doi.org/10.1016/j.compositesb.2020.108053.

(11) Denissen, W.; Winne, J. M.; Prez, F. E. D. Vitrimers: Permanent Organic Networks with Glass-like Fluidity. *Chem. Sci.* **2015**, *7* (1), 30–38. https://doi.org/10.1039/C5SC02223A.

(12) Schenk, V.; Labastie, K.; Destarac, M.; Olivier, P.; Guerre, M. Vitrimer Composites: Current Status and Future Challenges. *Mater. Adv.* **2022**, *3* (22), 8012–8029. https://doi.org/10.1039/D2MA00654E.

(13) Sharma, H.; Rana, S.; Singh, P.; Hayashi, M.; Binder, W. H.; Rossegger, E.; Kumar, A.; Schlögl, S. Self-Healable Fiber-Reinforced Vitrimer Composites: Overview and Future Prospects. *RSC Adv.* **2022**, *12* (50), 32569–32582. https://doi.org/10.1039/D2RA05103F.

(14) Wu, Y.; Wei, Y.; Ji, Y. Carbon Material/Vitrimer Composites: Towards Sustainable, Functional, and High-Performance Crosslinked Polymeric Materials. *Giant* **2023**, *13*, 100136. https://doi.org/10.1016/j.giant.2022.100136.

(15) Guerre, M.; Taplan, C.; Winne, J. M.; Prez, F. E. D. Vitrimers: Directing Chemical Reactivity to Control Material Properties. *Chem. Sci.* **2020**, *11* (19), 4855–4870. https://doi.org/10.1039/D0SC01069C.

(16) Krishnakumar, B.; Sanka, R. V. S. P.; Binder, W. H.; Parthasarthy, V.; Rana, S.; Karak, N. Vitrimers: Associative Dynamic Covalent Adaptive Networks in Thermoset Polymers. *Chemical Engineering Journal* **2020**, *385*, 123820. https://doi.org/10.1016/j.cej.2019.123820.

(17) Van Zee, N. J.; Nicolaÿ, R. Vitrimers: Permanently Crosslinked Polymers with Dynamic Network Topology. *Progress in Polymer Science* **2020**, *104*, 101233. https://doi.org/10.1016/j.progpolymsci.2020.101233.

(18) Yang, Y.; Pei, Z.; Zhang, X.; Tao, L.; Wei, Y.; Ji, Y. Carbon Nanotube–Vitrimer Composite for Facile and Efficient Photo-Welding of Epoxy. *Chem. Sci.* **2014**, *5* (9), 3486–3492. https://doi.org/10.1039/C4SC00543K.

(19) Lorwanishpaisarn, N.; Kasemsiri, P.; Srikhao, N.; Son, C.; Kim, S.; Theerakulpisut, S.; Chindaprasirt, P. Carbon Fiber/Epoxy Vitrimer Composite Patch Cured with Bio-Based Curing Agents for One-Step Repair Metallic Sheet and Its Recyclability. *Journal of Applied Polymer Science* **2021**, *138* (47), 51406. https://doi.org/10.1002/app.51406.

(20) Denissen, W.; De Baere, I.; Van Paepegem, W.; Leibler, L.; Winne, J.; Du Prez, F. E. Vinylogous Urea Vitrimers and Their Application in Fiber Reinforced Composites. *Macromolecules* **2018**, *51* (5), 2054–2064. https://doi.org/10.1021/acs.macromol.7b02407.

(21) Bai, L.; Zheng, J. Robust, Reprocessable and Shape-Memory Vinylogous Urethane Vitrimer Composites Enhanced by Sacrificial and Self-Catalysis Zn(II)–Ligand Bonds. *Composites Science and Technology* **2020**, *190*, 108062. https://doi.org/10.1016/j.compscitech.2020.108062.

(22) Luzuriaga, A. R. de; Martin, R.; Markaide, N.; Rekondo, A.; Cabañero, G.; Rodríguez, J.; Odriozola, I. Epoxy Resin with Exchangeable Disulfide Crosslinks to Obtain Reprocessable, Repairable and Recyclable Fiber-Reinforced Thermoset Composites. *Mater. Horiz.* **2016**, *3* (3), 241–247. https://doi.org/10.1039/C6MH00029K.

(23) Ji, F.; Liu, X.; Sheng, D.; Yang, Y. Epoxy-Vitrimer Composites Based on Exchangeable Aromatic Disulfide Bonds: Reprocessibility, Adhesive, Multi-Shape Memory Effect. *Polymer* **2020**, *197*, 122514. https://doi.org/10.1016/j.polymer.2020.122514.

(24) Liu, Y.-Y.; Liu, G.-L.; Li, Y.-D.; Weng, Y.; Zeng, J.-B. Biobased High-Performance Epoxy Vitrimer with UV Shielding for Recyclable Carbon Fiber Reinforced Composites. *ACS Sustainable Chem. Eng.* **2021**, *9* (12), 4638–4647. https://doi.org/10.1021/acssuschemeng.1c00231.

(25) Wang, Y.; Jin, B.; Ye, D.; Liu, Z. Fully Recyclable Carbon Fiber Reinforced Vanillin-Based Epoxy Vitrimers. *European Polymer Journal* **2022**, *162*, 110927. https://doi.org/10.1016/j.eurpolymj.2021.110927.

(26) Ruiz de Luzuriaga, A.; Markaide, N.; Salaberria, A. M.; Azcune, I.; Rekondo, A.; Grande, H. J. Aero Grade Epoxy Vitrimer towards Commercialization. *Polymers (Basel)* **2022**, *14* (15), 3180. https://doi.org/10.3390/polym14153180.

(27) Hao, C.; Liu, T.; Liu, W.; Fei, M.; Shao, L.; Kuang, W.; Simmons, K. L.; Zhang, J. Recyclable CFRPs with Extremely High Tg: Hydrothermal Recyclability in Pure Water and Upcycling of the Recyclates for New Composite Preparation. *J. Mater. Chem. A* **2022**, *10* (29), 15623–15633. https://doi.org/10.1039/D2TA03161B.

(28) Memon, H.; Wei, Y.; Zhang, L.; Jiang, Q.; Liu, W. An Imine-Containing Epoxy Vitrimer with Versatile Recyclability and Its Application in Fully Recyclable Carbon Fiber Reinforced Composites. *Composites Science and Technology* **2020**, *199*, 108314. https://doi.org/10.1016/j.compscitech.2020.108314.

(29) Si, H.; Zhou, L.; Wu, Y.; Song, L.; Kang, M.; Zhao, X.; Chen, M. Rapidly Reprocessable, Degradable Epoxy Vitrimer and Recyclable Carbon Fiber Reinforced Thermoset Composites Relied on High Contents of Exchangeable Aromatic Disulfide Crosslinks. *Composites Part B: Engineering* **2020**, *199*, 108278. https://doi.org/10.1016/j.compositesb.2020.108278.

(30) Xu, Y.; Dai, S.; Bi, L.; Jiang, J.; Zhang, H.; Chen, Y. Catalyst-Free Self-Healing Bio-Based Vitrimer for a Recyclable, Reprocessable, and Self-Adhered Carbon Fiber Reinforced Composite. *Chemical Engineering Journal* **2022**, *429*, 132518. https://doi.org/10.1016/j.cej.2021.132518.

(31) Markaide, N.; Luzuriaga, A. R. de; Gayraud, V.; Salaberria, A. M.; Rodríguez, M. E.; Walls, M. Design, Production and Characterization of High Performance 3R Composites Based on Dynamic Chemistry for the Aerospace Industry. *Revista de Materiales Compuestos* **2022**, *06-AEMAC en PROYECTOS EUROPEOS (2022)* (Num. 2-Monográfico Proyectos Europeos (2)). https://doi.org/10.23967/r.matcomp.2022.11.03.

(32) Kosarli, M.; Foteinidis, G.; Tsirka, K.; Markaide, N.; Ruiz de Luzuriaga, A.; Calderón Zapatería, D.; Weidmann, S.; Paipetis, A. S. 3R Composites: Knockdown Effect Assessment and Repair Efficiency via Mechanical and NDE Testing. *Applied Sciences* **2022**, *12* (14), 7269. https://doi.org/10.3390/app12147269.

(33) Builes Cárdenas, C.; Gayraud, V.; Rodriguez, M. E.; Costa, J.; Salaberria, A. M.; Ruiz de Luzuriaga, A.; Markaide, N.; Dasan Keeryadath, P.; Calderón Zapatería, D. Study into the Mechanical Properties of a New Aeronautic-Grade Epoxy-Based Carbon-Fiber-Reinforced Vitrimer. *Polymers* **2022**, *14* (6), 1223. https://doi.org/10.3390/polym14061223.

(34) Enns, J. B.; Gillham, J. K. Time–Temperature–Transformation (TTT) Cure Diagram: Modeling the Cure Behavior of Thermosets. *Journal of Applied Polymer Science* **1983**, *28* (8), 2567–2591. https://doi.org/10.1002/app.1983.070280810.

(35) Peng, X.; Gillham, J. K. Time–Temperature–Transformation (TTT) Cure Diagrams: Relationship between Tg and the Temperature and Time of Cure for Epoxy Systems. *Journal of Applied Polymer Science* **1985**, *30* (12), 4685–4696. https://doi.org/10.1002/app.1985.070301215.

(36) *Résines d'infusion HexFlow | Hexcel*. https://www.hexcel.com/Products/Prepregs-and-Resins/HexFlow-Infusion-Resins-for-Aerospace (accessed 2023-01-16).

(37) Matxain, J. M.; Asua, J. M.; Ruipérez, F. Design of New Disulfide-Based Organic Compounds for the Improvement of Self-Healing Materials. *Phys. Chem. Chem. Phys.* **2016**, *18* (3), 1758–1770. https://doi.org/10.1039/C5CP06660C.

(38) Guggari, S.; Magliozzi, F.; Malburet, S.; Graillot, A.; Destarac, M.; Guerre, M. Vanillin-Based Epoxy Vitrimers: Looking at the Cystamine Hardener from a Different Perspective. *ACS Sustainable Chem. Eng.* **2023**, *11* (15), 6021–6031. https://doi.org/10.1021/acssuschemeng.3c00379.

(39) Appleby-Thomas, G. J.; Hazell, P. J.; Stennett, C. The Variation in Lateral and Longitudinal Stress Gauge Response within an RTM 6 Epoxy Resin under One-Dimensional Shock Loading. *J Mater Sci* **2009**, *44* (22), 6187–6198. https://doi.org/10.1007/s10853-009-3859-z.

(40) Winter, H. H. Can the Gel Point of a Cross-Linking Polymer Be Detected by the G′ – G″ Crossover? *Polymer Engineering & Science* **1987**, *27* (22), 1698–1702. https://doi.org/10.1002/pen.760272209.

(41) Kamal, M. R.; Sourour, S. Kinetics and Thermal Characterization of Thermoset Cure. *Polymer Engineering & Science* **1973**, *13* (1), 59–64. https://doi.org/10.1002/pen.760130110.

(42) Karkanas, P. I.; Partridge, I. K.; Attwood, D. Modelling the Cure of a Commercial Epoxy Resin for Applications in Resin Transfer Moulding. *Polymer International* **1996**, *41* (2), 183–191. https://doi.org/10.1002/(SICI)1097-0126(199610)41:2<183::AID-PI621>3.0.CO;2-F.

(43) Karkanas, P. I.; Partridge, I. K. Cure Modeling and Monitoring of Epoxy/Amine Resin Systems. I. Cure Kinetics Modeling. *Journal of Applied Polymer Science* **2000**, *77* (7), 1419–1431. https://doi.org/10.1002/1097-4628(20000815)77:7<1419::AID-APP3>3.0.CO;2-N.

(44) Karkanas, P. I.; Partridge, I. K. Cure Modeling and Monitoring of Epoxy/Amine Resin Systems. II. Network Formation and Chemoviscosity Modeling. *Journal of Applied Polymer Science* **2000**, *77* (10), 2178–2188. https://doi.org/10.1002/1097-4628(20000906)77:10<2178::AID-APP11>3.0.CO;2-0.

(45) Navabpour, P.; Nesbitt, A.; Degamber, B.; Fernando, G.; Mann, T.; Day, R. Comparison of the Curing Kinetics of the RTM6 Epoxy Resin System Using Differential Scanning Calorimetry and a Microwave-Heated Calorimeter. *Journal of Applied Polymer Science* **2006**, *99* (6), 3658–3668. https://doi.org/10.1002/app.22869.

(46) Lagarias, J. C.; Reeds, J. A.; Wright, M. H.; Wright, P. E. Convergence Properties of the Nelder--Mead Simplex Method in Low Dimensions. *SIAM J. Optim.* **1998**, *9* (1), 112–147. https://doi.org/10.1137/S1052623496303470.

(47) D'Elia, R.; Dusserre, G.; Del Confetto, S.; Eberling-Fux, N.; Descamps, C.; Cutard, T. Cure Kinetics of a Polysilazane System: Experimental Characterization and Numerical Modelling. *European Polymer Journal* **2016**, *76*, 40–52. https://doi.org/10.1016/j.eurpolymj.2016.01.025.

(48) Flory, P. J. *Principles of Polymer Chemistry*; Cornell University Press, 1971.

(49) DiBenedetto, A. T. Prediction of the Glass Transition Temperature of Polymers: A Model Based on the Principle of Corresponding States. *Journal of Polymer Science Part B: Polymer Physics* **1987**, *25* (9), 1949–1969. https://doi.org/10.1002/polb.1987.090250914.

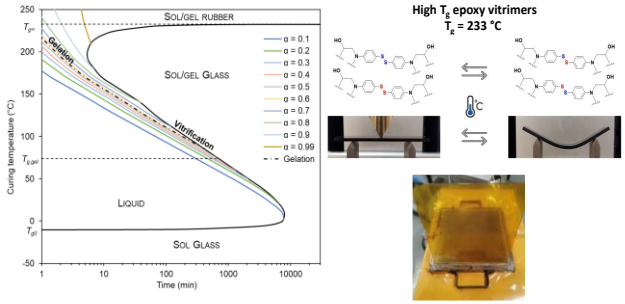

The construction of the first time-temperature-transformation (TTT) diagram for a vitrimer enabled the preparation of high Tg epoxy vitrimers (T_g >230 °C) by resin transfer moulding

Insert Table of Contents artwork here